diabetes®
American Diabetes Association®

Cardioprotection During Myocardial Infarction in Diabetic Cardiomyopathy

Sebastià Alcover, Sergi López, Lisaidy Ramos-Regalado, Natàlia Muñoz-García, Alex Gallinat, Rosa Suades, Lina Badimon, and Gemma Vilahur

Diabetes 2025;74(6):1021–1032 | https://doi.org/10.2337/db24-0510

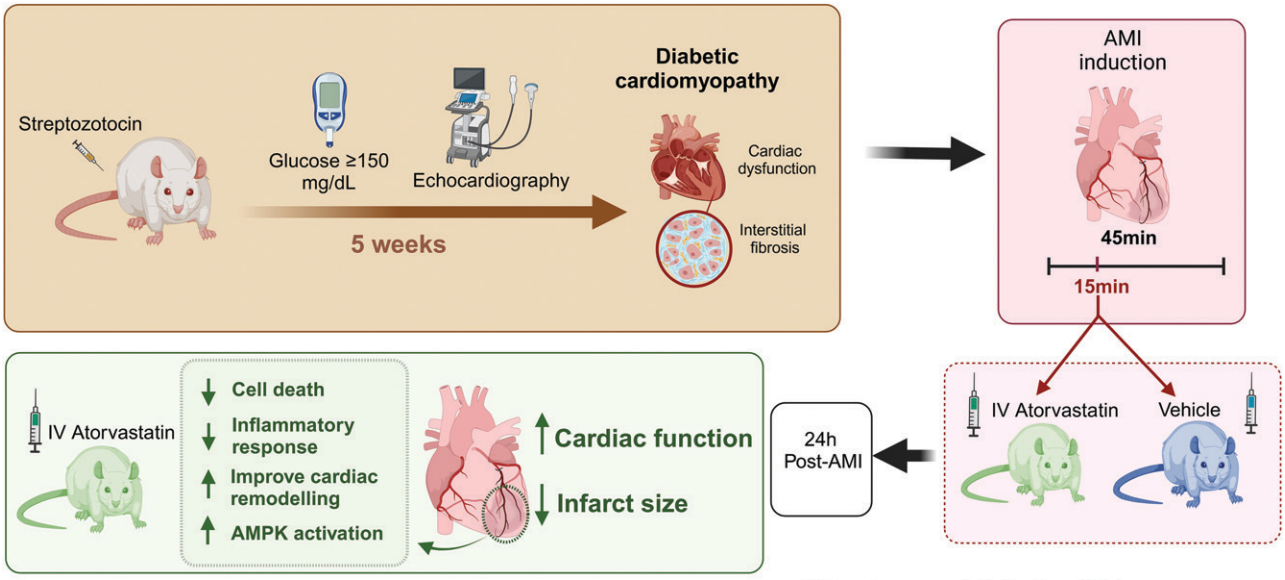

AMI, acute myocardial infarction; IV, intravenous.

Cardioprotection During Myocardial Infarction in Diabetic Cardiomyopathy

Sebastià Alcover,[1] Sergi López,[1] Lisaidy Ramos-Regalado,[1] Natàlia Muñoz-García,[1] Alex Gallinat,[1] Rosa Suades,[1] Lina Badimon,[1,2] and Gemma Vilahur[1,2]

Diabetes 2025;74:1021–1032 | https://doi.org/10.2337/db24-0510

Patients with diabetes are at an increased risk of diabetic cardiomyopathy (DCM) and acute myocardial infarction (AMI). Protecting the heart against AMI is more challenging in DCM than in nondiabetic hearts. We investigated whether intravenous (i.v.) atorvastatin administration during AMI exerts cardioprotection in DCM as seen in nondiabetic hearts. Sprague-Dawley rats were divided into streptozotocin-induced DCM and normoglycemic control groups. Our model of DCM rats exhibited interstitial fibrosis and cardiac dysfunction at 5 weeks. At this time point, all animals underwent AMI induction (coronary ligation for 45 min), receiving i.v. atorvastatin or vehicle during ischemia. Animals were reperfused and sacrificed 24 h later for myocardial infarct size analysis and cardiac tissue sampling. Echocardiography was performed. DCM vehicle rats had larger infarcts than normoglycemic vehicle-treated animals at a comparable area-at-risk. Intravenous atorvastatin reduced infarct size and preserved systolic function in both groups. Compared with vehicle animals, i.v. atorvastatin inhibited RhoA membrane translocation, induced AMPK phosphorylation, prevented apoptosis execution, and improved cardiac remodelling in the infarcted heart of both groups, whereas innate immune cell infiltration was further reduced in i.v. atorvastatin-treated DCM animals. The proven cardioprotective effectiveness of this i.v. statin formulation in the presence of DCM warrants its further development into a clinically therapeutic option.

ARTICLE HIGHLIGHTS

- Diabetic cardiomyopathy (DCM) significantly increases the risk of acute myocardial infarction and attenuates or abolishes the cardioprotective effects of several therapeutic approaches.
- Whether intravenous atorvastatin administration during ongoing acute myocardial infarction retains its cardioprotective potential in the presence of DCM was investigated.
- Intravenous atorvastatin during ischemia reduces infarct size and preserves cardiac function in DCM rats.
- The efficacy of this intravenous statin formulation in DCM supports its development as a viable therapeutic option for clinical use.

Diabetic cardiomyopathy (DCM), one of the most severe complications of diabetes, induces abnormalities in cardiac structure and function in the absence of other cardiovascular risk factors (hypertension, coronary artery disease, and atherosclerosis) (1,2). DCM pathogenesis includes macro- and microvascular alterations, cardiac inflammation, diffuse interstitial fibrosis, and overall adverse left ventricular (LV) remodelling (2).

Patients with diabetes have a two- to threefold higher relative risk of acute myocardial infarction (AMI), a worse prognosis post-AMI, and an increased risk of developing heart failure independently of age, risk factors, or comorbidities (3). Although several experimental studies have demonstrated the protective effect of pharmacological and mechanical interventions against AMI-related cardiac injury, these protective measures have not successfully translated to patients with diabetes (4,5). Metabolic alterations, such as hyperglycemia, insulin resistance, and diabetes, have been shown to enhance myocardial susceptibility to ischemic damage and markedly attenuate or even abolish the cardioprotective response afforded by ischemic and

[1]Sant Pau Research Institute (IR SANT PAU), Barcelona, Spain
[2]CiberCV, Institute of Health Carlos III, Madrid, Spain
Corresponding author: Gemma Vilahur, gvilahur@santpau.cat

Received 20 June 2024 and accepted 7 March 2025
This article contains supplementary material online at https://doi.org/10.2337/figshare.28565678.

pharmacological conditioning strategies (6). In the latter regard, conventional hypoglycemic drugs, such as metformin and thiazolidinediones, have shown limited cardioprotective efficacy across species (7). Conversely, the novel hypoglycemic drugs glucagon-like peptide 1 receptor agonists and sodium-dependent glucose cotransporter protein 2 inhibitors have been shown to exert infarct-sparing effects in diabetes at a preclinical (8) and clinical level (9,10), although the mechanisms behind remain unknown (6). However, to the best of our knowledge, no studies have addressed the cardioprotective potential of pharmacological interventions in the setting of AMI with a background of DCM, a diabetes-related complication characterized by pathological and functional features that differ from the diabetic heart.

We previously demonstrated in rodents (mice and rats) and preclinical (pigs) animal models that intravenous (i.v.) atorvastatin (IV-ATV) administration during ongoing ischemia significantly reduces myocardial damage, improves cardiac function, and limits adverse cardiac remodeling after AMI (11–15). Most importantly, such cardioprotective benefits persisted despite high plasma LDL-cholesterol levels (14). Chen et al. (16) demonstrated that pharmacological postconditioning with atorvastatin limited ischemia/reperfusion damage in a model of diabetes without cardiac impairment. Yet, whether IV-ATV is cardioprotective in the presence of DCM, a severe complication of diabetes associated with diastolic dysfunction and myocardial interstitial fibrosis, remains unknown. Therefore, we aimed to investigate whether IV-ATV administered during ischemia exerts cardioprotective effects in rats with established DCM.

RESEARCH DESIGN AND METHODS

Experimental approaches were reviewed and approved by the Institutional Animal Care and Use Committees (CEEA-IR, procedure no. 137) and authorized by the Animal Experimental Committee of the local government (Generalitat de Catalunya, Barcelona, Spain) by the Spanish law (RD 53/2013) and European Directive 2010/63/EU. In addition, the investigation conforms to the *Guide for the Care and Use of Laboratory Animals* published by the U.S. National Institutes of Health (NIH Publication No. 85-23, revised 1985), follows the Animal Research: Reporting of In Vivo Experiments (ARRIVE) guidelines 2.0 (17), and adheres to the practical guidelines for rigor and reproducibility in preclinical and clinical studies on cardioprotection (18,19). We are committed to the "3Rs" (Replacement, Reduction, and Refinement) principle and used the minimum of animals required to achieve statistical significance.

Animal Model of DCM

Male Sprague-Dawley rats (n = 24, weighing 250–300 g, 8–10 weeks old; Janvier Laboratory) were housed in standard cages (two/cage) and maintained under controlled temperature (24 ± 1°C) and humidity (55% ± 5%), with a 12-h light-dark cycle. The animals had ad libitum access to water and were fed regular chow (Teklad Global 14% Protein Rodent Maintenance Diet, Envigo). All animals were allowed to acclimatize 5 days before we conducted all baseline measurements. Thereafter, animals were randomly distributed into two groups: one group received a unique high dose of streptozotocin (STZ; 65 $mg{\cdot}kg^{-1}$ i.p.) to induce DCM (n = 12; 572201-1GM, Sigma-Aldrich, Burlington, MA), whereas the second group received an equal volume of sodium citrate buffer (normoglycemic control [NC] group, n = 12) (Supple>mentary Fig. 1) (20,21). Blood glucose levels were assessed within the first 48 h post-STZ administration (Accu-Chek Instant MO MG/DL, Roche Diabetes Care, Barcelona, Spain) to confirm the hyperglycemic condition (>150 $mg{\cdot}dL^{-1}$ fasting state).

Echocardiographic analyses were performed in all animals at baseline and at 3 and 5 weeks to follow-up on DCM development compared with NC. As detailed below, animals showed both diastolic and systolic dysfunction supporting the validity of this animal model of DCM (1, 22,23). To further validate our DCM rat model, we assessed interstitial fibrosis in another subgroup of animals (n = 16) that received a unique high dose of STZ (65 $mg{\cdot}kg^{-1}$ i.p.; n = 8) and were sacrificed at 5 weeks when cardiac dysfunction was evident. For this purpose, paraffin-embedded slices from the LV of DCM rats and of NC animals (n = 8) were processed for immunohistochemical analyses of collagen deposition (Masson's trichrome, Bio-Optica, Milan, Italy). Preparations were scanned by Pannoramic MIDI 1.17 (3DHISTECH) and with informatic program SlideViewer 2.7 (3DHISTECH) images, which were acquired and imported to ImageJ. Image-adjusted color threshold was performed to quantify cardiac fibrosis following same parameters (hue, 11–237; saturation, 0–254; brightness, 0–250). The collagen volume fraction was measured as a mean of five random fields per animal ([collagen positive area/total tissue area] × 100).

Blood Samples and Analyses

Rats were deeply anesthetized (Zoetis, Parsippany, NJ) at baseline, week 3, and 24 h post-AMI for blood withdrawal and serum obtention (TP010350, Everest-Tecnovet, Barcelona, Spain). The serum was stored at −80°C (24). We assessed triglycerides (GN 90125, RAL, Barcelona, Spain), total cholesterol (GN 20125, RAL), and HDL-cholesterol (GN 20525, RAL) levels. We also determined circulating levels of C-terminal propeptide of collagen α-1 chain (PICP) (ER0322-96T, FineTest, bioNova científica) and matrix metalloproteinase 1 (MMP1) (ER1158-96T, Fine-Test, bioNova científica) with their respective ELISA kits.

Transthoracic Echocardiography

All animals underwent transthoracic echocardiography to accurately assess cardiac function according to the indications provided by the European Society of Cardiology Working Group on Myocardial Function (25) by using a 30-MHz linear array transducer system (VEVO 2100, VisualSonics, Amsterdam, Netherlands).

LV structural analyses included LV anterior wall thickness in systole (LVAWs), LV anterior wall thickness in diastole (LVAWd), LV internal diameter in systole (LVIDs), LV internal diameter in diastole (LVIDd), interventricular septal thickness in systole (IVSs), interventricular septal thickness in diastole (IVSd), LV posterior wall thickness in systole (LVPWs), LV posterior wall thickness in diastole (LVPWd), LV systolic volume (LV Vs), LV diastolic volume (LV Vd), and relative wall thickness (RWT).

LV functional parameters included the analyses of the LV ejection fraction (LVEF), shortening fraction (SF), stroke volume (SV), and cardiac output (CO). In the case of large differences in body weight (BW), CO was normalized to body surface area (BSA) and expressed as the cardiac index (CI). $CI = CO \cdot BSA^{-1}$, $BSA = 9.8 \times BW^{2/3}$.

Peak velocity of early diastolic filling (*E* wave), late peak velocity of diastolic filling (*A* wave), isovolumetric relaxation time (IVRT), ejection time (ET), aortic ejection time (AET) and *E* wave-to- *A* wave ratio (E/A) were measured from the mitral inflow images to identify diastolic dysfunction. LV inflow pulsed-wave Doppler was also recorded.

Three representative cardiac cycles were evaluated for each determination, and heart rate (HR) was continuously monitored (26). Measurements were taken at baseline, week 3, week 5, and 24 h post-AMI.

AMI Model and Treatment

At week 5, rats were anesthetized by a subcutaneous injection of midazolam (0.5 $mg \cdot kg^{-1}$), alfaxalone (10 $mg \cdot kg^{-1}$), and buprenorphine (0.1 $mg \cdot kg^{-1}$). Rats were cannulated and connected to a rodent ventilator (Advanced Safety Ventilator, Harvard Apparatus, Holliston, MA), and a thoracotomy was performed at the fourth intercostal space (21). Pericardial tissue was removed, and myocardial infarct was performed by ligating the left anterior descending artery with a 5-0 silk suture (SQETW581, Everest-Tecnovet) (11). Myocardial infarction was confirmed by electrocardiogram visualization of the ST-elevation myocardial infarction pattern, and the infarcted myocardium showed as a pale pink color. Ischemia was maintained for 45 min. At 15 min of ischemia, the treated group received IV-ATV (2.75 $mg \cdot kg^{-1}$), whereas the vehicle animals received the same amount of vehicle (*N*,*N*-dimethylformamide) through the vein tail. The atorvastatin preparation used is a soluble atorvastatin calcium salt formulation for i.v. administration (patent PCT/EP2018/058158), and the doses of atorvastatin chosen were equivalent to the 40-mg oral dose of atorvastatin used in humans and converted to rat dosing according to body surface area (12).

After 45 min of ischemia, the coronary ligature was loosed, the chest was closed, and the skin was sewed with 5-0 silk (SQETW528H, Everest-Tecnovet). Rectal temperature was monitored and maintained during the experimental procedures within 37–38°C by the use of a heating plate (Rodent Surgical Monitor PLUS – Mouse and Rat, UNO Roestvatstaal BV, Zevenaar, Netherlands) (11).

Infarct Size Assessment

At 24 h post-AMI, all rats were anesthetized, cannulated, and connected to a rodent ventilator. The left anterior descending artery was reoccluded at the same point as AMI induction, and 3 mL of Evans Blue 1% (Evans Blue E2129-100G, Sigma-Aldrich) was perfused through the femoral vein. The heart was rapidly removed and washed with PBS at 4°C. The heart was cut into four slices with a 2-mm-thick section.

Two alternative slices were used for LV tissue collection for further molecular and histological studies of the infarcted myocardial zone. The remaining two slices were used for infarct size assessment with 1% triphenyl tetrazolium chloride (TTC) staining (27). The slices were photographed with a digital camera (Nikon D600, Tokyo, Japan) connected to a microscope (Technoscope Zeiss OPMI Pico S100, Jena, Germany) before and after TTC staining and analyzed using ImageJ. Infarct size was expressed as a percentage of the area at risk (AAR).

Myocardial Molecular Studies

Ischemic (jeopardized) myocardium, delineated by Evans Blue-negative staining, was collected and rapidly frozen in liquid nitrogen for mRNA and protein extraction following the indications provided by the supplier (TriPure, 11667165001, Sigma-Aldrich). We assessed the entire ischemic region as the scar had not yet developed 24 h post-AMI.

Assessment of Transcript Levels

RNA concentration was determined with a NanoDrop ND-1000 spectrophotometer (NanoDrop Technologies, Thermo Fisher Scientific, Waltham, MA), and purity was assessed by the A260-to-A280 ratio. cDNA was synthesized from 1 μg RNA with a cDNA reverse transcription kit (QIAGEN, Düsseldorf, Germany), and the resulting cDNA samples were amplified by RT-PCR with the following specific probes (Thermo Fisher Scientific) from Applied Biosystems (Carlsbad, CA): *1*) Ampk (*Ampk*; Rn00576935_m1), *2*) SiC2a4-Glut4 (*Glut4*; Rn01752377_m1), *3*) cysteine-aspartic acid protease 3 (*Caspase-3*; Rn00563902_m1), *4*) p53 (*P53*; Rn00755717_m1), *5*) collagen I (*Col1a1*; Rn0143848_m1), and *6*) collagen III (*Col3a1*; Rn01437681_m1). mRNA levels were normalized to the housekeeping gene *r18S* (Applied Biosystems).

Protein Expression and Activation

We assessed myocardial markers of *1*) cardiac metabolism: AMPK (1:500; ab3759-1001, Abcam, Cambridge, U.K.) and phosphorylated AMPK (p-AMPK) at threonine 172 (1:500; no. 2535, Cell Signaling, Danvers, MA); and *2*) glucose uptake: GLUT4 (1:500; sc-53566, Santa Cruz Biotechnology, Dallas, TX) and GLUT1 (1:500; no. 73015, Cell Signaling). The intensity of the Western blot bands was assessed with Chemi-Doc (Bio-Rad Life Science, Barcelona, Spain), and quantification was done with Quantity One Software (Bio-Rad Life Science). Normalization was performed against ponceau staining, and the intensity of

the bands was calculated by densitometry and expressed as arbitrary units (28).

Immunohistochemical Analyses

Paraffin-embedded slices from infarcted hearts of all animals were cut into 5-μm-thick serial sections (JUNG RM2055, Leica, Wetzlar, Germany) and processed for *1)* Masson's trichrome staining (as stated above); *2)* cardiomyocyte size assessment by hematoxylin (05-06004/L, Bio-Optica) and eosin (10-3001, Casa Álvarez, Madrid, Spain) staining (30 cardiomyocytes/image in five random fields); *3)* lipid peroxidation (a marker of ferroptosis) through the assessment of glutathione peroxidase (GPX)4 (1:200; ab125066, Abcam) (five images/sample; hue, 0–25; saturation, 30–110; brightness, 135–230); and *4)* innate immune cell recruitment by measuring total infiltrated macrophages (anti-CD68, 1:200; ab31630, Abcam), type 2 macrophages (anti-mannose receptor; 1:300; ab64693, Abcam), and neutrophils (anti-elastase; 1:200; ab68672-1001, Abcam) (positive cells were counted in 10 random fields).

Analyses of Apoptosis Execution by TUNEL Fluorescence Assay

Apoptosis in the infarcted heart was analyzed by TUNEL assay according to the manufacturer's instructions (Chemicon, Pittsburgh, PA). Images were recorded on a Leica inverted fluorescence confocal microscope (Leica TCS SP5-AOBS). Slices were viewed with HCX PL APO 63× oil/0.6-1.4 objective. Fluorescent images were acquired in a scan format of 1,024 × 1,024 pixels in a spatial data set (*x*, *y*, *z*) and were processed with the Leica Standard Software TCS-AOBS. Apoptosis rate was expressed in the mean of positive area (pixels) TUNEL-positive cells/microscopic field (∼100 cells), four random fields per heart.

Confocal Microscopy Analyses of RhoA and GLUT4 Activation

Staining of the plasmatic membrane (5 mg·mL^{-1}; C10046, Thermo Fisher Scientific) was performed in infarcted heart sections before RhoA (1:50; sc-418, Santa Cruz Biotechnology) and GLUT4 (1:50; sc-53566, Santa Cruz Biotechnology) immunochemistry following the manufacturer's instructions. Thereafter, colocalization of RhoA and GLUT4 in the plasma membrane (active forms) was evaluated by correlating the fluorescent signal represented in a two-dimensional cytofluorogram in which the overlapping is indicated in yellow. Only a central cloud along the *y*-*x*-axis of the cytofluorogram was selected and shown in yellow over images. The colocalization rate was calculated using colocalization area/area foreground ×100. Membrane colocalization analysis was performed in five random fields/sample.

Statistical Analysis

All analyses were performed blindly to both DCM conditions and treatment. Data are presented as mean ± SD. Normality was assessed with the Shapiro-Wilk test. When normality could be assumed, statistical differences between groups were analyzed by two-tailed *t* test (for comparisons between two groups), one-way ANOVA (for multiple groups), or two-way ANOVA (for multiple groups and two factors). The Tukey honestly significant difference post hoc test or the Bonferroni multiple comparisons test was performed to correct significance for multiple comparisons. Kruskal-Wallis rank sum test was performed when normality could not be assumed using GraphPad Prism software. The Pearson correlation coefficient provided the correlation of the intensity distributions between channels, and meanders overlap coefficient assessed the degree of colocalization. $P < 0.05$ was considered to indicate statistically significant differences.

Data and Resource Availability

All data generated or analyzed during this study are included in this published article and its supplementary information files.

RESULTS

Establishment of a Rat Model of STZ-Induced DCM

Glucose levels markedly rose 2 days post-STZ injection and remained high throughout the experimental study, and weight remained unchanged throughout the experimental period (Supplementary Fig. 2). Transthoracic echocardiography studies were performed at baseline and at 3 and 5 weeks post-STZ administration to verify the development of DCM. As shown in Fig. 1, DCM rats showed a significant dysfunction in systolic-related (Fig. 1*A*) and diastolic-related (Fig. 1*B*) parameters 3 weeks post-STZ injection (vs. NC animals) that persisted up to week 5. HR was also found to be depressed in DCM rats compared with NC rats (Fig. 1*C*). Hearts from DCM rats showed higher interstitial fibrosis than hearts from NC animals (Fig. 1*D*), further validating the DCM animal model.

IV-ATV Reduces Infarct Size in DCM Rats

Although there seemed to be a trend toward a reduction in the AAR in ATV-treated rats (NC and DCM) compared with their respective controls, *P* values were not statistically significant ($P < 0.71$ and $P < 0.43$, respectively), and no differences were detected among all animals per the AAR (Fig. 2). DCM-vehicle animals showed larger infarcts compared with NC-vehicle rats. Administration of IV-ATV early after AMI resulted in a significant and similar reduction in the size of infarction in NC and DCM animals compared with their vehicle counterparts (22 ± 7% vs. 23 ± 9%, respectively).

IV-ATV Inhibits RhoA Membrane Translocation in the Infarcted Myocardium

We first determined ATV-related inhibition of RhoA membrane translocation in the infarcted hearts. We detected a higher degree of RhoA translocation in the infarcted heart of DCM animals (vehicle and IV-ATV) than their NC counterparts

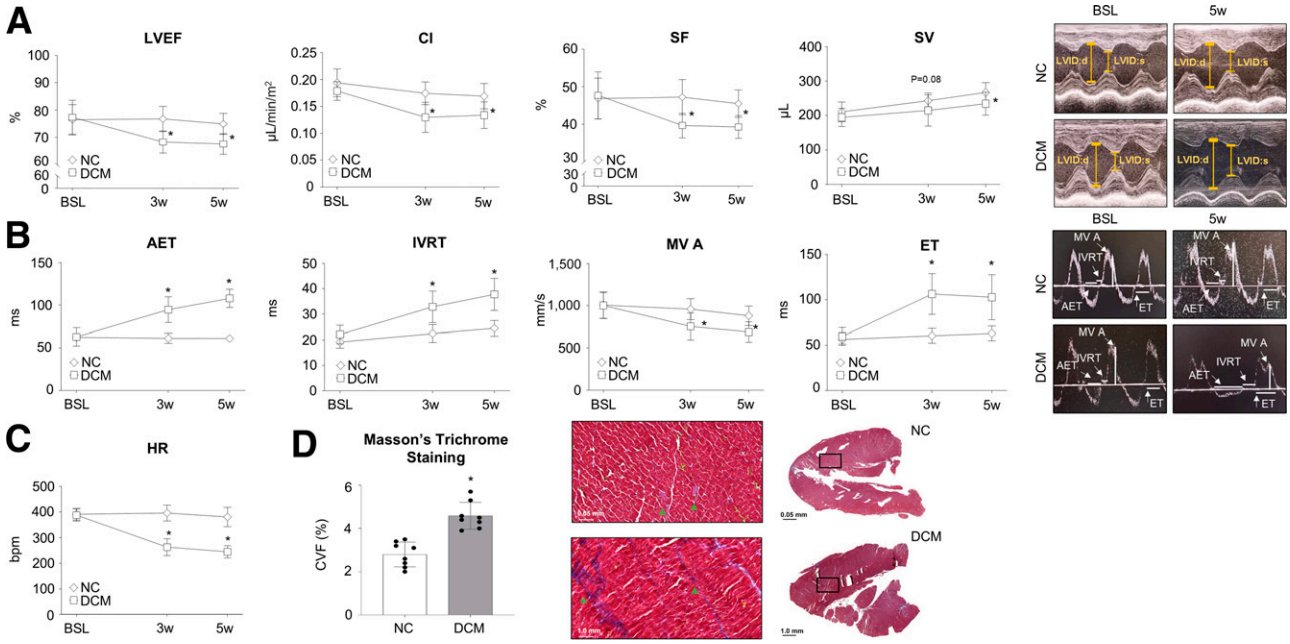

Figure 1—DCM characterization by cardiac echocardiography and fibrosis assessment. *A*: LV systolic-related parameters. *B*: LV diastolic-related parameters. *C*: HR (n = 12 animals/group in *A*, *B*, and *C*). bpm, beats per minute; BSL, baseline. *D*: Masson's trichrome staining (n = 8 animals/group). CVF, collagen volume fraction. Data are expressed as mean ± SD. *$P < 0.05$ vs. NC group.

(Fig. 3). IV-ATV administration significantly reduced RhoA translocation to the plasma membrane in both DCM and NC animals compared with their matching vehicle arm.

IV-ATV Preserves Systolic-Related Functional Parameters Post-AMI in DCM Rats

AMI induction for 45 min impaired LVEF, SF, and SV in all animal groups (vs. prior-AMI) (Fig. 4). Among non-treated animals, vehicle-DCM animals displayed a smaller relative impairment in all functional parameters than vehicle-NC animals. Of note, however, prior to AMI induction, LVEF (Fig. 1 and Fig. 4*A*), SF (Fig. 1 and Fig. 4*B*), and SV (Fig. 1 and Fig. 4*C*) were found to be significantly impaired in DCM animals compared with NC rats. IV-ATV markedly and similarly preserved systolic function in NC and DCM animals compared with vehicle-administered animals (Fig. 4). We could speculate that the vehicle-DCM animals displayed a smaller relative impairment in all functional parameters compared with the vehicle-NC animals likely because the vehicle-NC group showed better cardiac function before AMI induction, as shown in Fig. 1. Consequently, the vehicle-NC animals had a greater potential

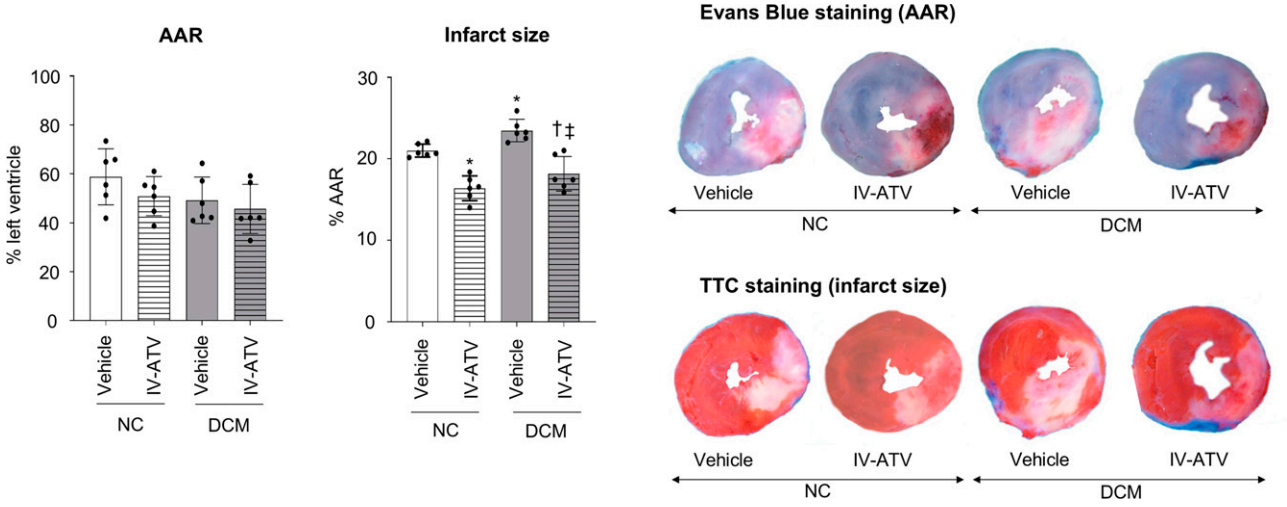

Figure 2—Infarct size assessment (n = 6 animals/group). Data are expressed as mean ± SD. *$P < 0.05$ vs. vehicle-NC; †$P < 0.05$ vs. vehicle-DCM; ‡$P < 0.05$ vs. IV-ATV NC.

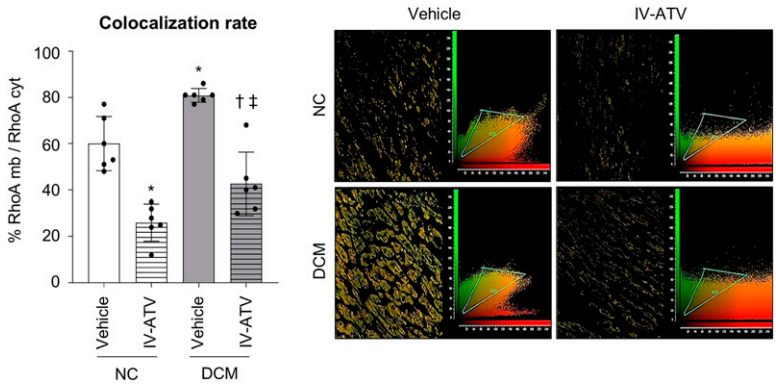

Figure 3—RhoA inhibition in the infarcted heart. Degree of colocalization rate and representative images. RhoA in the plasma membrane/RhoA in the cytoplasm (RhoA mb/RhoA cyt) (n = 6 animals/group). Data are expressed as mean ± SD. *$P < 0.05$ vs. vehicle-NC; †$P < 0.05$ vs. vehicle-DCM; ‡$P < 0.05$ vs. IV-ATV NC.

for myocardial impairment following AMI whereas vehicle-DCM animals had limited extent for further deterioration. IV-ATV administration also preserved LVAWs in both groups and LVIDs and LV Vs in NC animals (vs. vehicle-NC) (Supplementary Fig. 3). No differences were detected among all animals in other systolic and diastolic parameters (Supplementary Fig. 4).

IV-ATV Enhances Cardiac AMPK Activation in DCM Rats

Ampk transcript levels were found to be higher in the infarcted myocardium DCM-vehicle animals compared with NC-vehicle rats (Fig. 5*A*). Yet, no differences were detected as per the total AMPK protein content among NC and DCM animals (Fig. 5*B*). The degree of AMPK activation (and consequent ratio of p-AMPK to AMPK) was found to be significantly lower in DCM vehicle animals compared with NC-vehicle rats (Fig. 5*B*).

The administration of IV-ATV enhanced *Ampk* mRNA expression in the infarcted myocardium of NC animals compared with their vehicle counterparts, but no changes were observed in the DCM group. No changes were detected in AMPK protein expression after IV-ATV administration among both animal groups. In contrast, IV-ATV treatment was associated with a significant increase in AMPK activation and consequent ratio of p-AMPK to AMPK in both NC and DCM animals, although to a lower extent in the DCM group (vs. vehicle) (Fig. 5*B*).

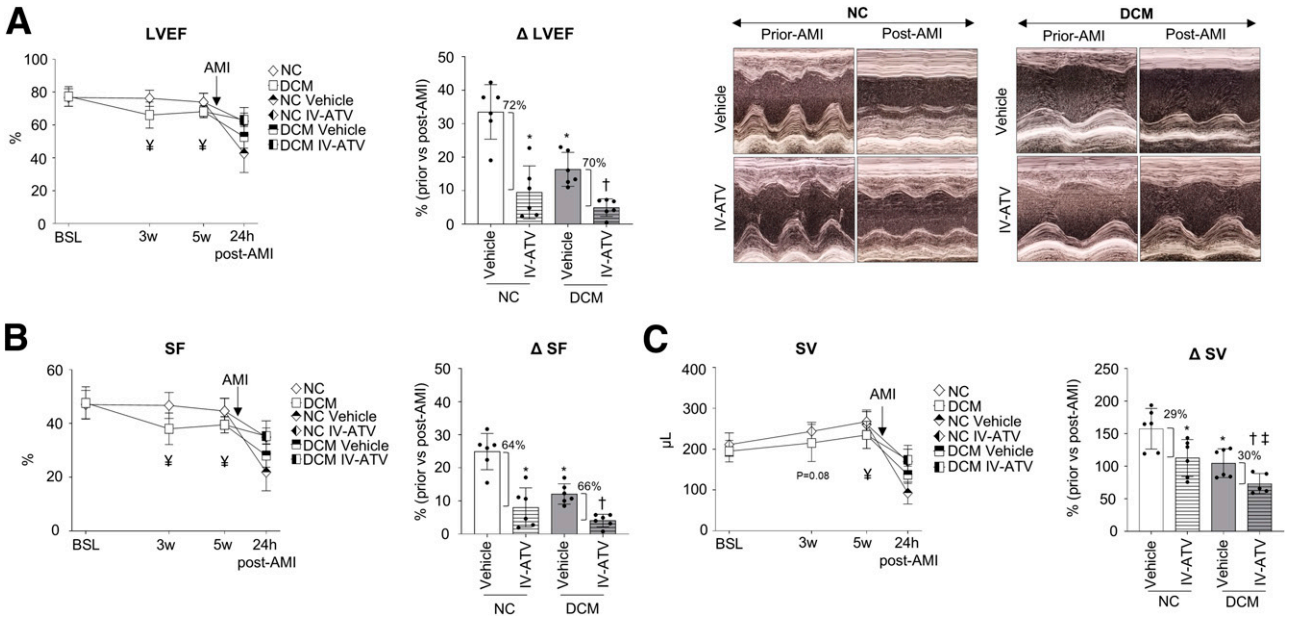

Figure 4—Echocardiography analysis of systolic-related parameters post-AMI induction. LVEF (*A*), SF (*B*), and SV (*C*). Δ: Relative impairment prior vs post-AMI (n = 6 animals/group). Data are expressed as mean ± SD. *$P < 0.05$ vs. vehicle-NC; †$P < 0.05$ vs. vehicle-DCM; ‡$P < 0.05$ vs. IV-ATV NC; ¥$P < 0.05$ vs. NC.

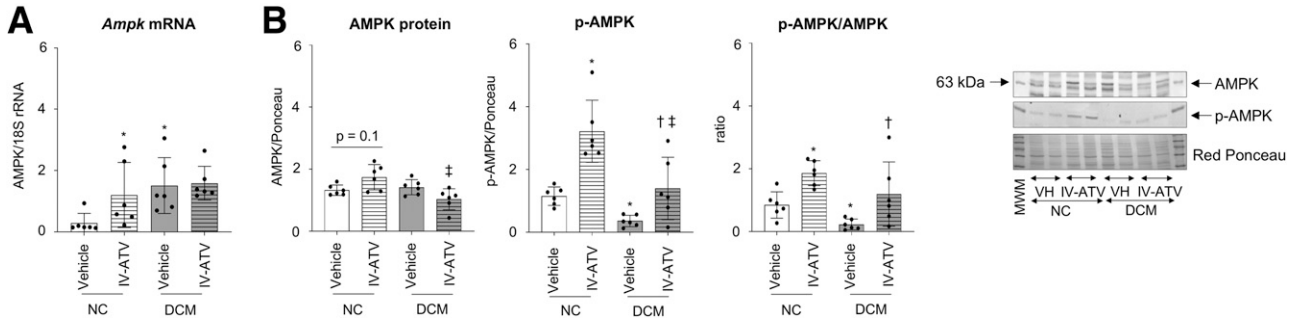

Figure 5—AMPK expression and activation in the infarcted heart. *A*: *Ampk* transcript levels. *B*: AMPK protein content and degree of activation (phosphorylation of threonine 172) (n = 6 animals/group). Data are expressed as mean ± SD. *$P < 0.05$ vs. vehicle-NC; †$P < 0.05$ vs. vehicle-DCM; ‡$P < 0.05$ vs. IV-ATV NC.

IV-ATV Exerts no Effect on Myocardial GLUT1 and GLUT4 Expression and GLUT4 Membrane Translocation

Altered glucose metabolism, a characteristic feature in diabetic conditions, has been demonstrated to contribute to the recovery of AMI (29). Accordingly, we examined whether IV-ATV administration affected GLUT1 and GLUT4 expression or GLUT4 membrane translocation. No differences were detected in *Glut4* transcript levels between NC-vehicle and DCM-vehicle animals in the infarcted heart (Supplementary Fig. 5*A*). In contrast, GLUT4 protein levels (Supplementary Fig. 5*B*) were found to be significantly reduced in DCM-vehicle animals compared with their NC counterparts. A comparable behavior was observed for GLUT1. Regarding GLUT4 membrane translocation, this was found to be significantly reduced in all DCM animals (Supplementary Fig. 5*C*). IV-ATV did not affect GLUT1 and GLUT4 protein levels or GLUT4 translocation in NC and DCM groups (Supplementary Fig. 5*B* and *C*).

IV-ATV Mitigates Apoptosis Execution in the Infarcted Myocardium of DCM Rats

P53 and *Caspase-3* transcript levels were found to be higher in the infarcted myocardial of DCM animals compared with NC (Fig. 6*A*). In line with the gene expression levels, TUNEL staining revealed higher apoptosis execution in the infarcted myocardium of DCM-vehicle animals compared with NC-vehicle rats (Fig. 6*C*). Yet, despite no changes detected in *Caspase-3* and *P53* transcript levels in IV-ATV treated animals, there was a 47% reduction in TUNEL staining in IV-ATV NC animals and a 76% reduction in IV-ATV DCM rats.

We also assessed GPX4, an enzyme that prevents lipid peroxidation and subsequent ferroptosis. No differences in GPX4 detection were observed among all animal groups (Fig. 6*C*).

Impact of IV-ATV on Cardiac Innate Immune Cell Infiltration

DCM-vehicle animals showed a clear trend (P = 0.08) toward a higher (40%) neutrophil infiltration and a significant increase in macrophage content in the infarcted heart compared with NC-vehicle rats (Fig. 7*A* and *B*). IV-ATV administration largely limited inflammatory cell recruitment (64% and 21% reduction in neutrophil and macrophage, respectively) in the infarcted region of DCM rats, whereas it exerted no significant effect on NC rats. On the other hand, lower amounts of type 2 macrophages were detected in the infarcted myocardium of all DCM animals compared with their NC counterparts, and IV-ATV treatment resulted in higher detection levels compared with the vehicle counterparts (Fig. 7*B*).

IV-ATV Limits Adverse Cardiac Remodelling

DCM-vehicle animals showed an increased *Col3a1* mRNA level in the infarcted heart compared with the NC-vehicle group. No differences were detected according to *Col1a1* gene expression levels, and DCM animals showed lower circulating levels of PIPC. MMP1 levels did not differ between NC and DCM animals (Fig. 8*A*–*C*). At a histological level, DCM-vehicle animals showed higher fibrosis detection in the infarcted heart than their NC-vehicle counterparts (Fig. 8*D*).

The impact of IV-ATV treatment on fibrosis differed between NC and DCM animals. Among NC animals, IV-ATV increased cardiac transcript levels of *Col1a1* and *Col3a1,* enhanced PICP circulating levels, and lowered MMP1 concentrations (Fig. 8*A*–*C*). In contrast, among DCM animals, IV-ATV resulted in lower expression of *Col1a1*, *Col3a1*, and PICP and higher MMP1 levels (Fig. 8*A*–*C*). In line with these findings, higher fibrosis was detected in the evolving scar of IV-ATV NC animals compared with their vehicle NC counterparts (Fig. 8*D*), whereas IV-ATV administration led to lower fibrosis deposition in the DCM hearts.

No differences in cardiomyocyte size were observed between the NC and DCM at 5 weeks after STZ administration (Supplementary Fig. 6*A*) or among groups at 24 h post-AMI (Supplementary Fig. 6*B*).

Impact of IV-ATV on Plasma Lipid Levels

Triglycerides, total cholesterol, and HDL-cholesterol levels were higher in the DCM animals compared with the NC rats at 3 weeks, an effect that persisted up to 24 h post-AMI (Supplementary Table 1). IV-ATV administration exerted no changes in all tested lipid parameters.

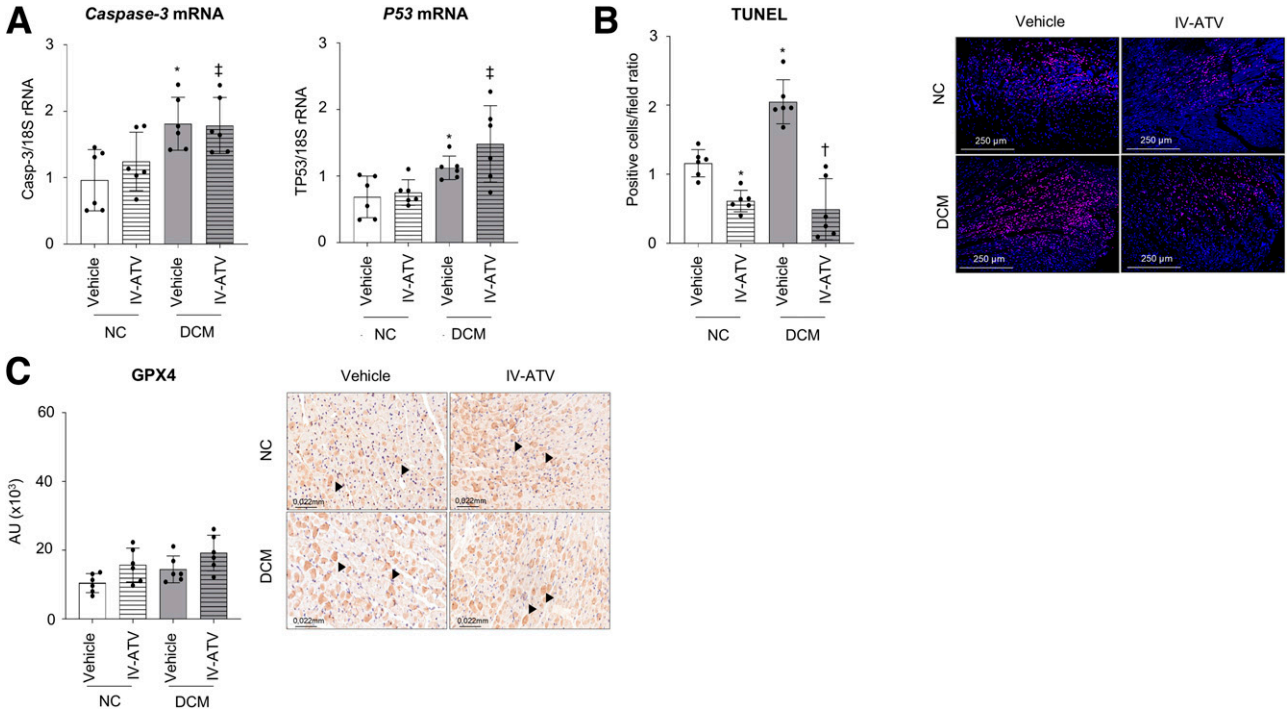

Figure 6—Cell death assessment in the infarcted heart. *A*: Transcript levels of *P53* and *Caspase-3*. *B*: TUNEL staining. Scale bar = 250 µm. *C*: GPX4 (arrowheads) cardiac expression (n = 6 animals/group). Scale bar = 0.022 mm. AU, arbitrary units. Data are expressed as mean ± SD. *$P < 0.05$ vs. NC-vehicle; †$P < 0.05$ vs. DCM-vehicle; ‡$P < 0.05$ vs. NC IV-ATV.

DISCUSSION

The failure to translate novel cardioprotective approaches to the clinical setting has been partly attributed to comorbid conditions (3,30). Additionally, the excessive reactive oxygen species production, persistent low-grade inflammatory state, and dysfunctional response to insulin that characterizes diabetes have been suggested to interfere with key cardioprotective signaling pathways, making diabetic animal models resistant to certain mechanical and pharmacological cardioprotective interventions (6,22,31). We have soundly demonstrated in small- and large-animal models that IV-ATV during ongoing AMI robustly reduces cardiac damage and improves LV remodelling and that such benefits remain despite high plasma LDL-cholesterol levels (11,12,14).

We now demonstrate that the cardioprotection conferred by IV-ATV administered during ischemia persists in DCM rats. So far, there is still no animal model that recapitulates the full complexity of DCM, yet our STZ-induced rat model of DCM mimics both the dysfunctional phenotype that characterizes human DCM developing both diastolic and systolic dysfunction (1,22,23) (evidenced by an increase in IVRT and *A* peak and a decrease in LVEF and SF, respectively) and the presence of diffuse myocardial fibrosis (6).

Inhibition of HMG-CoA reductase reduces mevalonate synthesis and the subsequent formation of farnesyl pyrophosphate and geranyl pyrophosphate. Both farnesyl pyrophosphate and geranyl pyrophosphate anchor intracellular proteins (such as the small G protein RhoA) through prenylation, ensuring its translocation into the cell membrane. Once activated, RhoA has been shown to trigger detrimental effects on the cardiovascular system. RhoA activity has been noted to increase in various cardiovascular disease models, including DCM (32). In line with these findings, we detect a higher degree of RhoA membrane translocation in DCM animals than in NC animals. Yet, IV-ATV was able to mitigate RhoA activation in the infarcted heart to a comparable extent in all animals regardless of the DCM condition. RhoA inhibition by fasudil in mice has been shown to promote liver kinase B1 activity, leading to p-AMPK (33). AMPK plays a crucial role in modulating cardiac metabolism in the presence of myocardial ischemia (34). Several studies have demonstrated the negative impact of hyperglycemia on AMPK expression and activity (35,36), worsening cardiac adaptation to an ischemic insult (37). In the current study and in agreement with previous findings (38), we evidence that the DCM condition significantly reduces AMPK activation to comparable levels found in infarcted hearts. In addition, we also demonstrate higher apoptosis execution in the infarcted region of nontreated DCM rats. DCM pathophysiology is characterized by a higher caspase-3 and p53 activation (39), which in our study, might have been further challenged by AMI-induction as we and others have previously shown (40,41). Although no differences were observed according to GPX4 content, this does not allow us to exclude potential differences in GPX4 activity. Further studies are needed to ascertain the contribution of ferroptosis to overall cell death.

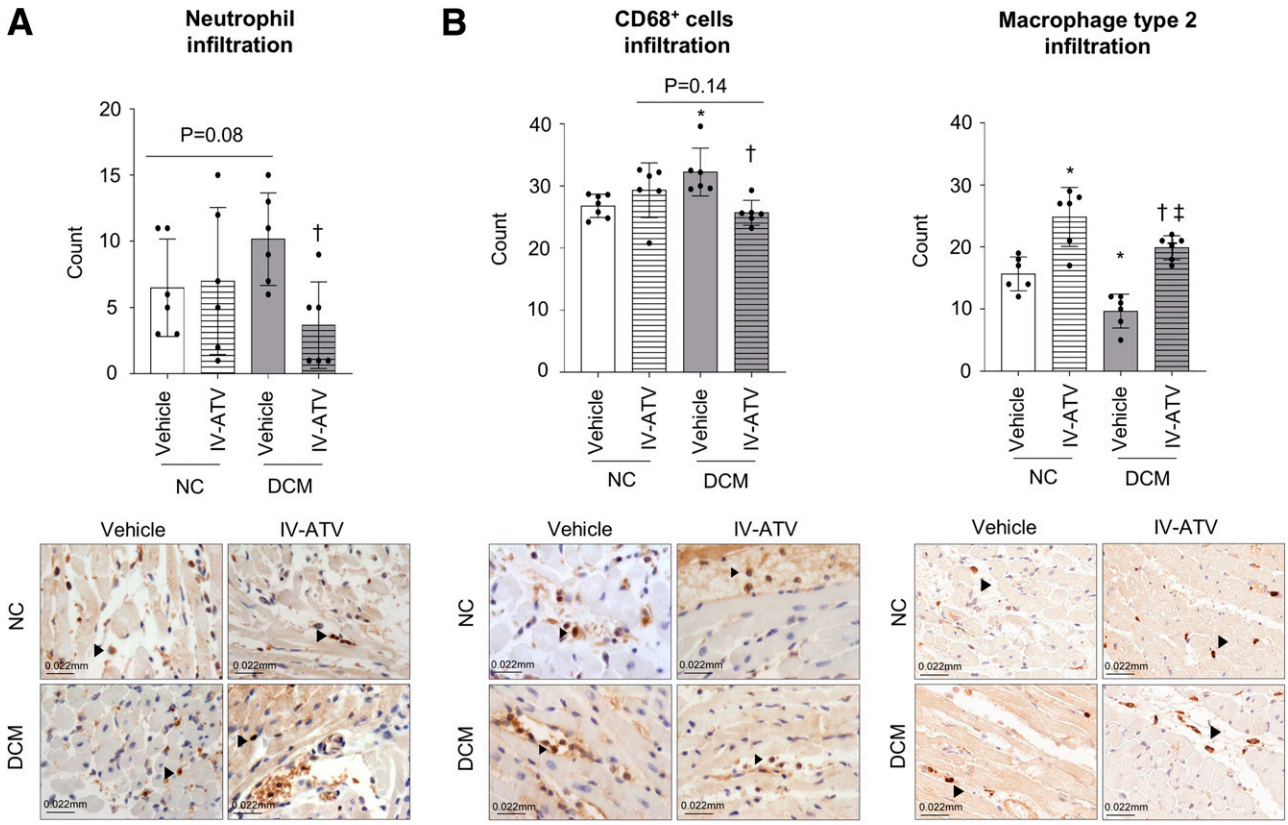

Figure 7— Innate immune cell detection in the infarcted heart. *A*: Neutrophil infiltration. Arrowheads (black) depict the innate immune cells. Scale bar(s), 0.022 mm. *B*: CD68$^+$ cells and macrophage type 2 infiltration (n = 6 animals/group). Scale bar(s), 0.022 mm. Data are expressed as mean ± SD. *$P < 0.05$ vs. NC-vehicle; †$P < 0.05$ vs. DCM-vehicle; ‡$P < 0.05$ vs. NC IV-ATV.

Altogether, the higher degree of RhoA translocation and apoptosis execution in combination with a lower ratio of p-AMPK observed in the jeopardized myocardium may contribute to explain the larger infarcts observed in nontreated DCM rats compared with their NC counterparts. The presence of hypertension and dyslipidemia has been shown to lead to larger infarcts (42,43). More recently, in isolated rat hearts, DCM has shown impairing effects on ischemia/reperfusion injury, reducing the effects of preconditioning (44). We prove in vivo the impairing effects of DCM on heart structure and function and how AMI further impairs cardiac performance. Most importantly, we demonstrate that administration of IV-ATV during ongoing ischemia can revert the DCM-induced deleterious effects on cardiac function and how both AMPK activation and cell death are likely involved in limiting the final size of infarction. We previously demonstrated, by using a selective AMPK inhibitor, a causal association between IV-ATV administration and AMPK activation. On the other hand and in line with our previous work (11), IV-ATV treatment likely reduces apoptosis execution despite the absence of detectable modifications in *Caspase-3* and *P53* transcript levels. This conclusion is supported by the observed decrease in TUNEL staining and our previous findings in pigs, where IV-ATV led to a reduced activity of both caspase-3 and p53 in the infarcted heart (11, 45).

Beyond AMPK, glucose transporters (particularly GLUT1 and GLUT4) have been shown to play critical roles in the metabolic response to myocardial damage. In this regard, cardiac tolerance under ischemia largely depends upon glycolysis, and glucose-insulin-potassium infusions have been shown to limit cardiac damage and improve recovery after AMI (46). We observed the expected reduction in GLUT1 and GLUT4 expression and GLUT4 translocation to the cytoplasmatic membrane in DCM rats, likely due to impaired insulin sensitivity (13). Yet, IV-ATV administration did not affect GLUT1 and GLUT4 content or activation, likely excluding any effects of IV-statin on cardiac glucose uptake. IV-ATV did not exert any effect on plasma lipid levels in line with our previous findings (12,14). Cholesterol reduction by statins requires prolonged inhibition of liver HMG-CoA reductase, making a single i.v. infusion insufficient to achieve meaningful lipid level reductions.

We further assessed the impact of IV-ATV on cardiac innate immune cell response, considering the key role of inflammation in the pathogenesis of both DCM- and AMI-triggered cardiac damage (39). As such, we observed a clear trend toward higher neutrophil and macrophage recruitment in the infarcted area in DCM rats compared with NC rats, which was significantly attenuated in those animals treated with IV-ATV. We previously demonstrated in hypercholesterolemic pigs the ability of IV-ATV to limit

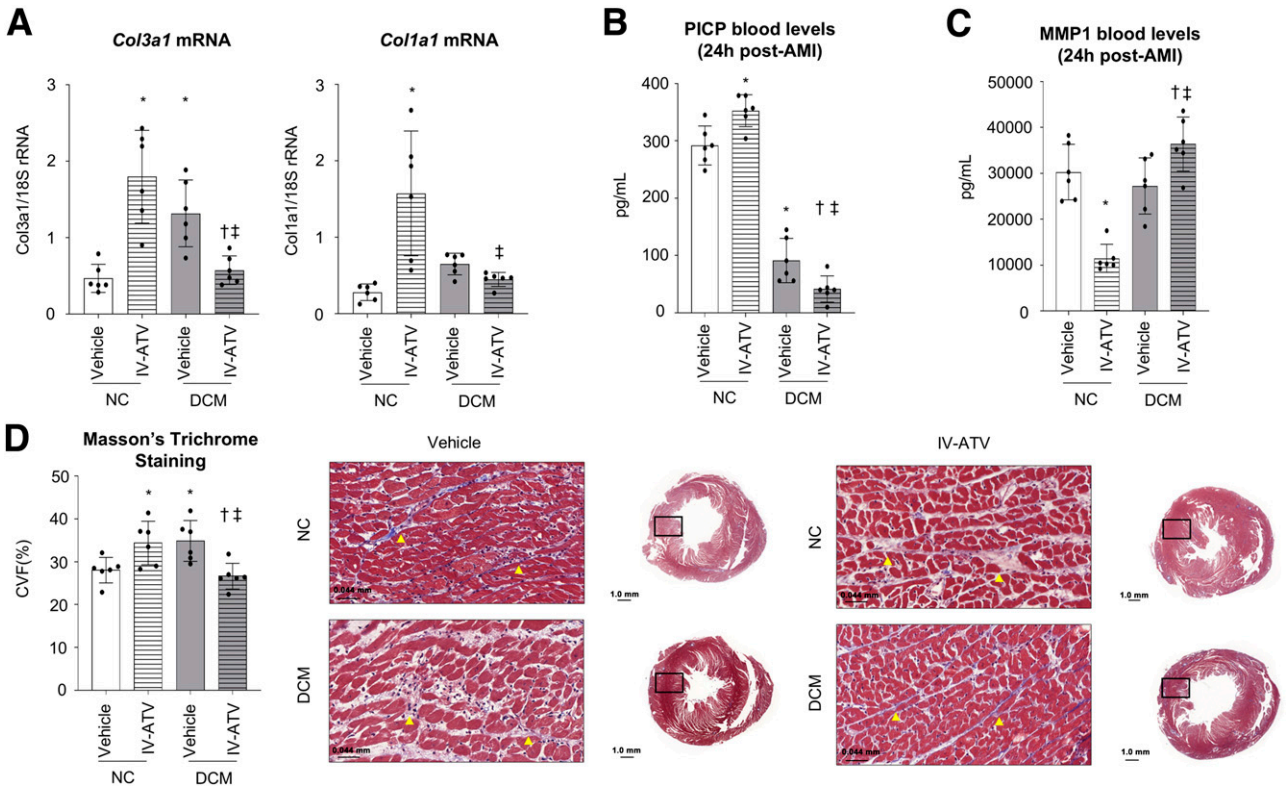

Figure 8—Fibrotic markers in the infarcted heart. *A*: *Col3a1* and *Col1a1* transcript levels. *B*: PICP circulating levels. *C*: MMP1. *D*: Masson's trichrome staining (n = 6 animals/group). Scale bar(s), 0.044 mm, 1.0 mm. Data are expressed as mean ± SD. *$P < 0.05$ vs. NC-vehicle; †$P < 0.05$ vs. DCM-vehicle; ‡$P < 0.05$ vs. NC IV-ATV.

ischemia-induced neutrophil infiltration (11) and to diminish reperfusion-induced peripheral blood mononuclear cell activation at 3 days post-AMI (12). We now provide evidence that IV-ATV not only prevents local cardiac infiltration of innate immune cells but also enhances the presence of type 2 macrophages (anti-inflammatory phenotype) found to be diminished in DCM hearts (47).

Moreover, we studied the effect of IV-ATV on the cardiac fibrotic remodelling process (2). Interestingly, a dual effect of IV-ATV was observed depending on the pathological background. Our observations in a whole allow us to speculate that whereas IV-ATV favored reparative fibrosis in the forming scar of NC animals (higher collagen content and lower MMP1 levels), it limited further fibrous tissue deposition in an already fibrotic DCM heart (48) overall, supporting a beneficial effect of IV-ATV on ventricular remodeling. Finally, in line with previous studies, we did not observe an increase in cardiomyocyte size during the development of DCM at 5 weeks (49,50) and IV-statin induced no changes in cardiomyocyte size post-AMI in the infarcted heart, in line with our recent findings in hyperlipidemic pigs (45).

Study Limitations

Our study has some limitations. First we could not evaluate the impact of sex on the study because Sprague-Dawley female rats are resistant to diabetes induced by STZ administration (51).

Second, by design we only evaluated the short-term efficacy of the IV-ATV intervention and did not assess longer periods. However, we proved before in a preclinical animal model of hypercholesterolemia that the acute benefits of IV-ATV intervention persist in the chronic phase post-AMI attenuating LV adverse remodeling at 42 days.

Third, our model of DCM is based on a type 1 diabetes model following a single injection of STZ and does not recapitulate the features of type 2 diabetes (e.g., inadequate weight gain over time and concurrence with other comorbidities) (20). Whether our observations can be translated to a setting of type 2 diabetes remains to be assessed.

Finally, although the operations were not blinded to the treatment arm, all subsequent analyses presented in this manuscript were conducted under blinded conditions.

Conclusions

IV-ATV administered during ongoing ischemia limits infarct size and preserves cardiac function post-MI despite the presence of DCM. These benefits are associated with enhanced AMPK activation, reduced apoptosis execution, lower innate immune cell recruitment, and improved cardiac remodeling in the infarcted heart (graphical abstract). This novel approach holds promise in the clinical setting

and deserves to be investigated in patients suffering from AMI with a background of DCM.

Acknowledgments. The authors thank the valuable help and support of L. Casaní, E. Peña, M.A. Velasco, I. Rodríguez, J. Oriol, P. Catalina, and M.A. Cánovas.

This article is part of the PhD studies of S.A. for the Doctorate in Biomedicine at the University of Barcelona.

Funding. This work was supported by the SEC/FEC-INV-TRL 20/015 funded by the Spanish Society of Cardiology (G.V.). It was also funded by grant PID2021-128891OB-I00 (to G.V.) and grant PID2019-107160RB-I00 (to L.B), PLEC2021-007664–Unión Europea NextGenerationEU/PRTR (to G.V.), and grant M-ERA-NET-3/PCI2023-143431–EU Horizon 2020 (to G.V.) funded by MCIN/AEI/10.13039/501100011033 and Fondo Europeo de Desarrollo Regional (FEDER) A way of making Europe; and the Generalitat of Catalunya-Secretaria d'Universitats i Recerca del Departament d'Economia i Coneixement de la Generalitat (2017SGR1480 to L.B.), and 2016PROD00043 (Agencia Gestión Ayudas Universitarias Investigación: AGAUR).

Duality of Interest. L.B. and G.V. are the authors of the patent (PCT/EP2018/058158) that includes the use of statins for intravenous administration and founders and shareholders of Ivestatin S.L. No other potential conflicts of interest relevant to this article were reported.

Author Contributions. S.A. contributed to the design, analysis, interpretation of data, and drafting of the manuscript. S.L. and N.M.-G. contributed to the interpretation of data and drafting of the manuscript. L.R., A.G., and R.S. performed analysis and interpretation of data. L.B. revised the paper critically for important intellectual content. G.V. was key in the conception and design of the study, revising it critically for important intellectual content, for funding the study and for the final approval of the manuscript submitted. L.B. and G.V. are authors of the patent. All authors read and approved the final manuscript. G.V. is the guarantor of this work and, as such, had full access to all the data in the study and takes responsibility for the integrity of the data and the accuracy of the data analysis.

References

1. Lezoualc'h F, Badimon L, Baker H, et al. Diabetic cardiomyopathy: the need for adjusting experimental models to meet clinical reality. Cardiovasc Res 2023;119:1130–1145

2. Tan Y, Zhang Z, Zheng C, Wintergerst KA, Keller BB, Cai L. Mechanisms of diabetic cardiomyopathy and potential therapeutic strategies: preclinical and clinical evidence. Nat Rev Cardiol 2020;17:585–607

3. Rawshani A, Rawshani A, Franzén S, et al. Mortality and cardiovascular disease in type 1 and type 2 diabetes. N Engl J Med 2017;376:1407–1418

4. Schulz R, Andreadou I, Hausenloy DJ, Ferdinandy P. Risk factors, comorbidities, and co-medications in cardioprotection: importance for translation. Br J Pharmacol 2020;177:5249–5251

5. Badimon L, Mendieta G, Ben-Aicha S, Vilahur G. Post-genomic methodologies and preclinical animal models: chances for the translation of cardioprotection to the clinic. Int J Mol Sci 2019;20:514

6. Ferdinandy P, Andreadou I, Baxter GF, et al. Interaction of cardiovascular nonmodifiable risk factors, comorbidities and comedications with ischemia/reperfusion injury and cardioprotection by pharmacological treatments and ischemic conditioning. Pharmacol Rev 2023;75:159–216

7. Techiryan G, Weil BR, Palka BA, Canty JM. Effect of intracoronary metformin on myocardial infarct size in swine. Circ Res 2018;123:986–995

8. Bose AK, Mocanu MM, Carr RD, et al. Glucagon-like peptide 1 can directly protect the heart against ischemia/reperfusion injury. Diabetes 2005;54:146–151

9. Cesaro A, Gragnano F, Paolisso P, et al. In-hospital arrhythmic burden reduction in diabetic patients with acute myocardial infarction treated with SGLT2-inhibitors: Insights from the SGLT2-I AMI PROTECT study. Front Cardiovasc Med 2022;9:1012220

10. Wong SY, Lee ARYB, Sia AHJ, et al. Effects of glucagon-like peptide-1 receptor agonist (GLP-1RA) on cardiac structure and function: a systematic review and meta-analysis of randomized-controlled trials. Cardiovasc Drugs Ther 2024;38:371–389

11. Mendieta G, Ben-Aicha S, Casani L, Badimon L, Sabate M, Vilahur G. Molecular pathways involved in the cardioprotective effects of intravenous statin administration during ischemia. Basic Res Cardiol 2019;115:2

12. Mendieta G, Ben-Aicha S, Gutiérrez M, et al. Intravenous statin administration during myocardial infarction compared with oral post-infarct administration. J Am Coll Cardiol 2020;75:1386–1402

13. Ritchie RH, Abel ED. Basic mechanisms of diabetic heart disease. Circ Res 2020;126:1501–1525

14. Vilahur G, Casani L, Peña E, et al. HMG-CoA reductase inhibition prior reperfusion improves reparative fibrosis post-myocardial infarction in a preclinical experimental model. Int J Cardiol 2014;175:528–538

15. Badimon L, Vilahur G. Prevention or reduction of ischemia-related damage. U.S. patent 11052136B2. 14 March 2017

16. Chen L, Cai P, Cheng Z, Zhang Z, Fang J. Pharmacological postconditioning with atorvastatin calcium attenuates myocardial ischemia/reperfusion injury in diabetic rats by phosphorylating GSK3β. Exp Ther Med 2017;14:25–34

17. Percie Du Sert N, Ahluwalia A, Alam S, et al. Reporting animal research: explanation and elaboration for the ARRIVE guidelines 2.0. PLoS Biol 2020;18:e3000411

18. Bøtker HE, Hausenloy D, Andreadou I, et al. Practical guidelines for rigor and reproducibility in preclinical and clinical studies on cardioprotection. Basic Res Cardiol 2018;113:391

19. Lindsey ML, Bolli R, Canty JM, et al. Guidelines for experimental models of myocardial ischemia and infarction. Am J Physiol Heart Circ Physiol 2018;314:H812–H838

20. Furman BL. Streptozotocin-induced diabetic models in mice and rats. Curr Protoc Pharmacol 2015;70:5.47.1–5.47.20

21. Li H, Liu Z, Wang J, et al. Susceptibility to myocardial ischemia reperfusion injury at early stage of type 1 diabetes in rats. Cardiovasc Diabetol 2013;12:133–111

22. Mihm MJ, Seifert JL, Coyle CM, Bauer JA. Diabetes related cardiomyopathy time dependent echocardiographic evaluation in an experimental rat model. Life Sci 2001;69:527–542

23. Joffe II, Travers KE, Perreault-Micale CL, et al. Abnormal cardiac function in the streptozotocin-induced non-insulin-dependent diabetic rat: noninvasive assessment with Doppler echocardiography and contribution of the nitric oxide pathway. J Am Coll Cardiol 1999;34:2111–2119

24. Hao L, Lu X, Sun M, Li K, Shen L, Wu T. Protective effects of L-arabinose in high-carbohydrate, high-fat diet-induced metabolic syndrome in rats. Food Nutr Res 2015;59:28886

25. Zacchigna S, Paldino A, Falcão-Pires I, et al. Towards standardization of echocardiography for the evaluation of left ventricular function in adult rodents: a position paper of the ESC Working Group on Myocardial Function. Cardiovasc Res 2021;117:43–59

26. Liu Y, Lei S, Gao X, et al. PKCβ inhibition with ruboxistaurin reduces oxidative stress and attenuates left ventricular hypertrophy and dysfunction in rats with streptozotocin-induced diabetes. Clin Sci (Lond) 2012;122:161–173

27. Yang S, Abbott GW, Gao WD, Liu J, Luo C, Hu Z. Involvement of glycogen synthase kinase-3β in liver ischemic conditioning induced cardioprotection against myocardial ischemia and reperfusion injury in rats. J Appl Physiol (1985) 2017;122:1095–1105

28. Luquero A, Vilahur G, Casani L, Badimon L, Borrell-Pages M. Differential cholesterol uptake in liver cells : a role for PCSK9. FASEB J 2022;36:e22291

29. Dambrova M, Zuurbier CJ, Borutaite V, Liepinsh E, Makrecka-Kuka M. Energy substrate metabolism and mitochondrial oxidative stress in cardiac ischemia/reperfusion injury. Free Radic Biol Med 2021;165:24–37

30. Ferdinandy P. Myocardial ischaemia/reperfusion injury and preconditioning: effects of hypercholesterolaemia/hyperlipidaemia. Br J Pharmacol 2003;138:283–285
31. Nakamura K, Miyoshi T, Yoshida M, et al. Pathophysiology and treatment of diabetic cardiomyopathy and heart failure in patients with diabetes mellitus. Int J Mol Sci 2022;23:3587
32. Liu X, Liu Y, Tang L, Du C. Inhibition of farnesyl pyrophosphate synthase alleviates cardiomyopathy in diabetic rat. Cell Cycle 2023;22:666–679
33. Noda K, Nakajima S, Godo SRho-kinase inhibition ameliorates metabolic disorders through activation of AMPK pathway in mice. PLoS One 2014;9:e110446
34. Zuurbier CJ, Bertrand L, Beauloye CR, et al. Cardiac metabolism as a driver and therapeutic target of myocardial infarction. J Cell Mol Med 2020; 24:5937–5954
35. Coughlan KA, Valentine RJ, Ruderman NB, Saha AK. Nutrient Excess in AMPK downregulation and insulin resistance. J Endocrinol Diabetes Obes 2015;1:1008
36. Ruderman NB, Carling D, Prentki M, Cacicedo JM. AMPK, insulin resistance, and the metabolic syndrome. J Clin Invest 2013;123:2764–2772
37. Entezari M, Hashemi D, Taheriazam A, et al. AMPK signaling in diabetes mellitus, insulin resistance and diabetic complications: a pre-clinical and clinical investigation. Biomed Pharmacother 2022;146:112563
38. Xie Z, He C, Zou M-H. AMP-activated protein kinase modulates cardiac autophagy in diabetic cardiomyopathy. Autophagy 2011;7:1254–1255
39. Dillmann WH. Diabetic cardiomyopathy. Circ Res 2019;124:1160–1162
40. Santos-Gallego CG, Requena-Ibáñez JA, Picatoste B, et al. Cardioprotective effect of empagliflozin and circulating ketone bodies during acute myocardial infarction. Circ Cardiovasc Imaging 2023;16:e015298
41. Vilahur G, Juan-Babot O, Peña E, Oñate B, Casaní L, Badimon L. Molecular and cellular mechanisms involved in cardiac remodeling after acute myocardial infarction. J Mol Cell Cardiol 2011;50:522–533
42. Mølgaard S, Faricelli B, Salomonsson M, Engstrøm T, Treiman M. Increased myocardial vulnerability to ischemia-reperfusion injury in the presence of left ventricular hypertrophy. J Hypertens 2016;34:513–523; discussion 523
43. Vilahur G, Casani L, Juan-Babot O, Guerra JM, Badimon L. Infiltrated cardiac lipids impair myofibroblast-induced healing of the myocardial scar post-myocardial infarction. Atherosclerosis 2012;224:368–376
44. Kurian GA, Ansari M, Prem PN. Diabetic cardiomyopathy attenuated the protective effect of ischaemic post-conditioning against ischaemia-reperfusion injury in the isolated rat heart model. Arch Physiol Biochem 2023;129:711–722
45. Vilahur G, Ben-Aicha S, Gutiérrez M, et al. Cardioprotection exerted by intravenous statin at index myocardial infarction event attenuates cardiac damage upon recurrent infarction. Cardiovasc Res 2025;121:283–295
46. Toedebusch R, Belenchia A, Pulakat L. Diabetic cardiomyopathy: impact of biological sex on disease development and molecular signatures. Front Physiol 2018;9:453–414
47. Sheridan A, Wheeler-Jones CPD, Gage MC. The immunomodulatory effects of statins on macrophages. Immuno 2022;2:317–343
48. Muller M, Trocme C, Lardy B, Morel F, Halimi S, Benhamou PY. Matrix metalloproteinases and diabetic foot ulcers: the ratio of MMP-1 to TIMP-1 is a predictor of wound healing. Diabet Med 2008;25:419–426
49. Al-Rasheed NM, Al-Rasheed NM, Hasan IH, et al. Simvastatin ameliorates diabetic cardiomyopathy by attenuating oxidative stress and inflammation in rats. Oxid Med Cell Longev 2017;2017:1092015
50. Sun S, Yang S, Zhang N, et al. Astragalus polysaccharides alleviates cardiac hypertrophy in diabetic cardiomyopathy via inhibiting the BMP10-mediated signaling pathway. Phytomedicine 2023;109:154543
51. Furman BL. Streptozotocin-induced diabetic models in mice and rats. Curr Protoc 2021;1:e78